Transportation Research Part B 149 (2021) 118–137

Contents lists available at ScienceDirect

Transportation Research Part B

journal homepage: www.elsevier.com/locate/trb

24thd International Symposium on Transportation and Traffic Theory, ISTTT 24, 24–26 July 2021, Beijing, China

Enforcing optimal routing through dynamic avoidance maps

Ludovic Leclercq*, Andres Ladino, Cécile Becarie

Université Gustave Eiffel, ENTPE, LICIT, Lyon, 69675, France

ARTICLE INFO

Article history:
Received 22 December 2020
Revised 19 April 2021
Accepted 4 May 2021

Keywords:
Optimal route guidance
Urban traffic control
Perimeter control
Avoidance maps
System optimum
Cooperative control

ABSTRACT

This paper presents a new concept for operating traffic management at a sizeable urban scale. The overall principle is to partition the network into multiple regions, where traffic conditions should remain optimal. Instead of monitoring the inflow, like for perimeter control, deviations in regional mean speed compared to a reference value are transformed into avoidance levels by a centralized controller. That information is broadcasted to vehicles through a public avoidance map. The onboard navigation systems then interpret this map to deliver individual route guidance according to the avoidance levels. In that way, the concept tends to distribute vehicles in the network optimally while preserving privacy. In addition to the controller parameters itself, three other critical parameters define the system: the safety distance, the controller time horizon, and the region sizes. Thorough sensitivity analysis leads to the optimal setting. The concept is proven effective using microsimulation for both a Manhattan and a realistic network. The total travel time is improved by about 15% when traffic is severely congested compared to the uncontrolled case. In the meantime, the mean individual travel distance increase for rerouted vehicles is kept below 10%. Those results have been obtained with a simple decentralized reactive control framework, i.e., an individual proportional feedback system independently governs each region. More advanced formulations introducing cooperation between the regions are also tested. In a nutshell, this paper is a proof of concept for a new control system that appears both practical and valuable to alleviate congestion in urban areas.

© 2021 The Authors. Published by Elsevier B.V.

Peer-review under responsibility of the scientific committee of the 24th International Symposium on Transportation and Traffic Theory

© 2021 The Author(s). Published by Elsevier Ltd.
This is an open access article under the CC BY-NC-ND license
(http://creativecommons.org/licenses/by-nc-nd/4.0/)

1. Introduction

Traffic engineers are looking for traffic management strategies acting at a broader scale than classical local traffic signal control to improve traffic conditions over the whole city area. Two main options have emerged: perimeter control and optimal route guidance. Perimeter control, e.g. (Keyvan-Ekbatani et al., 2012, 2013, 2015; Geroliminis et al., 2013; Haddad and Shraiber, 2014; Haddad, 2017a; J. 2017b) has proven very successful to alleviate congestion within an area by monitoring the

* Corresponding author.
E-mail address: ludovic.leclercq@univ-eiffel.fr (L. Leclercq).

https://doi.org/10.1016/j.trb.2021.05.002
0191-2615/© 2021 The Author(s). Published by Elsevier Ltd. This is an open access article under the CC BY-NC-ND license
(http://creativecommons.org/licenses/by-nc-nd/4.0/)

entry flow at the perimeter. While such proofs are mainly theoretical or based on simulation studies, first implementations in the field exist like in Zürich (Switzerland). Züritraffic system adapts traffic signal settings at the city perimeter depending on the real-time inner traffic conditions. The most appealing parts of perimeter control are that (i) it requires few data to operate, mainly the monitoring of inner traffic conditions, and (ii) control actions can be implemented by coordinating existing traffic signal settings. The main drawback is that it generates queues at the perimeter, merely moving congestion from the inner city to city gates or the suburbs. Some studies have proposed solutions to that issue by considering external queues in the objective function (Hajiahmadi et al., 2015; Yang et al., 2016; Kouvelas et al., 2017; Nie and Cassidy, 2019) or by implementing multiple control cordons to distribute the congestion, e.g. (Aboudolas and Geroliminis, 2013; Ramezani et al., 2015; Keyvan-Ekbatani et al., 2015; Haddad and Mirkin, 2017; Ampountolas et al., 2017).

Optimal route guidance appears as the best option on paper. It can detour vehicles from congested areas while creating no additional queues as strategic decisions are taken at the individual level in advance to the congestion, e.g. (Yildirimoglu et al., 2015, 2018; Ding et al., 2017; Sirmatel and Geroliminis, 2018). However, unless autonomous cars are massively deployed in the field, optimal routing strategies mainly resort to the goodwill of users. Unfortunately, they can quickly figure out when the proposed alternative is against their interests. It is the classical antagonism between user and system optimum. (Munoz and Laval, 2006) clearly showed for the one-destination problem that a system optimum routing strategy could significantly reduce the total time traveled by all users. They have to start deviating from the bottleneck much sooner than what a routing system based on actual travel times would advise. Note that solving the optimal routing problem for all users is not only very challenging in practice but requires massive computational resources and extensive real-time data collection as we should at least know all user destinations. Privacy concerns may raise if a central intelligence has to gather such data to ensure efficient traffic management. It certainly explains why optimal collective route guidance strategies are not yet implemented in the field. Another reason is that most of the actual routing systems/technologies, e.g., Google Maps, Waze, Tomtom traffic, are developed by tech companies that focus their business on user services and then indirectly promote user equilibrium, i.e., shortest path in time for their users.

In this paper, we propose a new concept that comes up with the best of the two large-scale control options: multi-perimeter and optimal route guidance. The network is first partitioned into regions like in perimeter control. Instead of limiting inflows, the system individually prevents some users from entering the areas by advising them alternative itineraries. Two hierarchical stages guarantee privacy by design. The first stage resorts to a centralized controller. It monitors the traffic states in each region and derives specific avoidance levels, i.e., the fraction of users that should avoid an area (0: full avoidance, 1: full availability). The partitioning and the avoidance levels define a map, which is broadcasted to circulating vehicles at each control time step, e.g., 3–10 min. The second stage is decentralized at the vehicle's level. Each of them first transforms the global avoidance map into a private one by performing Bernoulli trials in each crossed region. Each private avoidance map now defines which regions are unavailable for each user. The itineraries are then accordingly modified by the onboard GPS. It can be done automatically every time a new global avoidance map is pushed. Note that this concept can also be alternatively designed as a stand-alone component directly embedded in existing navigation maps. Operators have to agree to change their usual user-centered routing discipline by alternatives that comply with the avoidance maps. Public authorities may need to enforce adequate regulations or agree to pay the operators to improve the traffic conditions in their territories.

In any case, this concept would require updating navigation systems to account for avoidance map instructions, which only requires software updates. Of course, we have to convince (i) the system operators to implement the option, which can require new regulation, and (ii) the users to follow the guidance. This paper proves that the new concept is promising if these two conditions hold. It focuses on the design of the central controller and the overall assessment of the system using a micro-simulation as the plant model (ground-truth reference). A central feature of our concept is that privacy is guaranteed by design as the control center has no access to the individual trajectories and only monitor the network states. Each vehicle acts according to the regulation in a decentralized manner without sharing information.

This paper is organized as follows. Section 2 presents the concept in detail and the control methodology. Section 3 describes the different case studies and highlight the research questions (performance assessment and sensitivity analysis). Section 4 presents all numerical results and the central insights of this research. Section 5 provides conclusions and a short discussion.

2. Concept and methodology

2.1. Concept

Fig. 1 proposes an overview of the concept. A preliminary step is to partition the network into regions, see. Fig. 1a. We will not discuss this step here, and the readers are referred to the extensive literature about urban network partitioning/clustering, e.g. (Ji and Geroliminis, 2012; Saeedmanesh and Geroliminis, 2016; 2017; Lopez et al., 2017). Particular attention should be paid to compactness, like in perimeter control applications, but also region sizes. Regions should also not include key network links in terms of connectivity, e.g., a bridge or a tunnel, as users should always have alternative paths to reach their destination when a region is temporally inaccessible. This requirement is usually not restrictive for urban networks as they are highly redundant. However, critical links, when existing, should be excluded from the partitioning. They are always available and not included in the control framework. Finally, note that the region perimeters are invariant

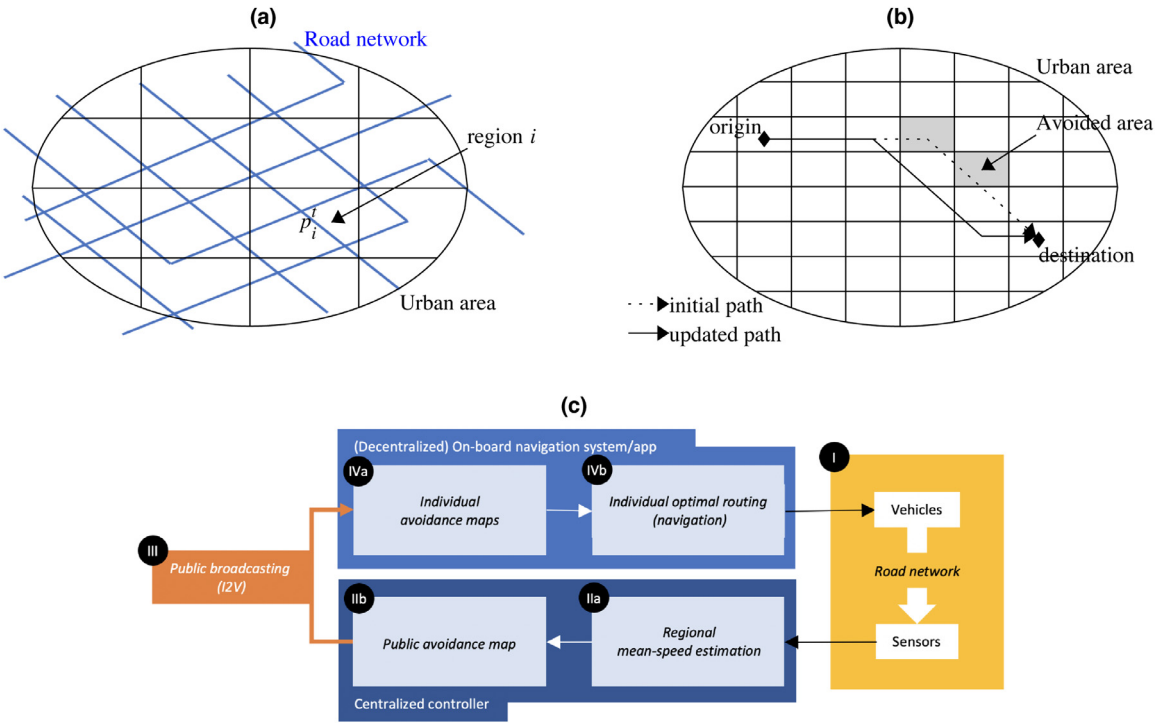

Fig. 1. The control concept (a) public avoidance maps; (b) individual avoidance map and impacts of the vehicle trajectory; (c) overall sketch.

in time, and the partitioning is done before tuning the centralized controller. Further studies will consider dynamic and automatic network clustering.

For a given network partition into N regions, the centralized controller aims to determine, for each region i, the optimal avoidance level p_i^t during the next time horizon $[t, t + T]$. p_i^t represents the fraction of users that should avoid region i while their regular path (shortest path in time) crosses it. The list of $\{p_i^t\}$ values and the partitioning define the public avoidance map, which remains active until the next controller update at time $t + T$. The controller inputs are the spatial mean-speeds monitored in each region during the last time interval $[t - T, t]$, see Fig. 1c. Speed estimation is out of the scope of this study, but robust and accurate methods exist in the literature when probe vehicles are available, e.g. (Leclercq et al., 2014; Van Erp et al., 2017). Loop detectors can be used too but with lower accuracy.

T is an essential parameter of the system and should be set cautiously. If T is short, it may end up with too frequent re-routing requests. Users may find it annoying, which will lower the compliance rate in the end. If T is high, the controller is ineffective as it is not adapting fast enough to changes in the network state. Our experience with the concept leads us to set T to a default value of 3 min, but the system sensitivity to this parameter will be further studied in Section 4. Multiple control frameworks can be integrated into the centralized controller. Here, we restricted ourselves to reactive strategies. Predictive ones have been proven superior in terms of overall performance, e.g., (Aboudolas and Gerolimins, 2013; Yang et al., 2016) in the context of multi-region perimeter control strategies. However, they require more advanced settings and can be very sensitive to the accuracy of the embedded prediction model. Our focus here is to demonstrate the validity of the new concept for optimal route guidance. We prefer to put methodological efforts on estimating the optimal parameter settings and investigating the benefits from cooperation between regions. All details are provided in the next subsection.

The public avoidance map is broadcasted to users via different channels (I2V, 4G/5G networks). Such an asymmetric communication system is essential to ensure privacy by design. Users will act according to the map without sharing information with the centralized controller. It only uses aggregate information from network monitoring. When a vehicle receives an updated map, its navigation system performs the following operations, see also Fig. 1b:

- Calculating the shortest-path in time to destination without any regional access restrictions. This path is the *regular path* the navigation system would advise in the absence of the control strategy;
- Identifying the different regions crossed by the regular path where $p_i^t > 0$. In each such region, a Bernoulli trial is done following p_i^t. Every time the outcome is positive, the related region is labeled as inaccessible for this particular vehicle;
- Calculating the final path. It corresponds to the shortest-path in time, now considering the regional restrictions.

Bernoulli trials transform the public avoidance map into individual avoidance maps specific to each vehicle. Individual maps have only two possible labels per region: available or unavailable. The law of large number guarantees that the fraction of successful outcomes from repetitive Bernoulli trials, which corresponds here to the effective fraction $p^*{}_i^t$ of users

avoiding region i, converges to the probability of success ${p_i}^t$, when the number of draws is sufficient. In practice, the control system is active when the network is saturated, which means the number of vehicles and thus of draws is high. This does not guarantee perfect convergence but provides some confidence in the proposed solution. Other factors can influence the difference between ${p^*}_i{}^t$ and ${p_i}^t$. The most obvious is the penetration and compliance rates, as some vehicles may not have a compatible navigation system or users may purposely choose not to follow the guidance. In this paper, we assume that those both rates are equal to 1. Also, we have to introduce a safety distance d between a vehicle and the next crossed region border. If the actual distance is below this threshold d, the navigation system will ignore the next region's avoidance order. This prevents the vehicle from hazardous maneuvers as the alternative path may require significant local deviation from the regular path when a vehicle is approaching an inaccessible region. Finally, some vehicles, e.g., buses and taxis, may have been granted full permission while driving on the network and are then not considered during the trials. All these factors act in the same direction and reduce ${p^*}_i{}^t$ compared to ${p_i}^t$. A solution to improve the system efficiency is to overweight ${p_i}^t$ by a proportional factor that roughly compensates these effects. This option is not implemented in this paper but may be considered in further studies to deploy the system in the field.

Fig. 1c proposes an overview of how the overall concept works. The control framework is presented in the next subsection. The system has three key parameters that can influence its performance: the control time horizon, T, the region size and the safety distance, d. We will investigate their impacts among the numerical test cases in Section 4 through sensitivity analysis.

2.2. Control framework

This section describes how the centralized controller derives the avoidance levels ${p_i}^t$ in each region i from the current spatial mean speed observations ${u_i}^t$. Formally, the speed observations are aggregated over the previous controller time horizon $[t - T, t]$, while the avoidance levels are applied for the next $[t, t + T]$. We opt for a straightforward control framework that is efficient and easy to implement in practice: a decentralized reactive control scheme. The framework is decentralized as each region has its independent controller that acts based on the local observations only. It is reactive as we only use the current speed observations to derive the control actions, i.e., the avoidance levels. Predictive strategies, e.g. (Geroliminis et al., 2013; Haddad, J., Shraiber, 2014; Sirmatel and Geroliminis, 2018), determine the optimal control actions by forecasting the future states of the system. They are usually more accurate and exhibit superior stability performances at the price of higher computational burden that is sometimes not compatible with real-time applications. In this paper, we do not aim to make a methodological contribution in control theory but rather to assess our new large-scale urban control concept. It is the main reason we kept the control framework simple and opted for a proportional controller in each region.

A reference speed ${u_i}^*$ characterizes the optimal traffic conditions in each region, see Section 2.3. When ${u_i}^t > {u_i}^*$, the traffic is in free-flow, and no control is required. So, we define the error term ${e_i}^t$ as the positive difference between ${u_i}^*$ and ${u_i}^t$, i.e., ${e_i}^t = \max(0, {u_i}^* - {u_i}^t)$. The proportional controller transforms this observed error into the control action ${p_i}^t$ using a proportionality factor K_p.

$$(P): \quad p_i^t = \min\left(K_p e_i^t, 1 - \varepsilon\right) \tag{1}$$

In this paper, we assume that K_p values are identical for all regions. Avoidance levels should fall between 0 and 1. As the errors are positive, ${p_i}^t \geq 0$. In particular, ${p_i}^t$ is equal to 0 when the traffic conditions are free-flow. The larger the errors, the higher the avoidance levels, meaning that the entry restrictions are made more severe. Note that a maximal bound equal to $1\text{-}\varepsilon$ is introduced for ${p_i}^t$ values. So, a region is never entirely inaccessible. In this paper, we set ε to 5%. An essential consideration in this framework is that providing specific avoidance levels to a region is a way to modify its spatial speed in a finite timeframe. We already mentioned why the control system might lead to observed avoidance levels ${p^*}_i{}^t$ lower than the controller requests ${p_i}^t$. One more reason is the absence of coordination between vehicles rerouting actions as the decisions are fully decentralized. So, there is no guaranty that the number of vehicles that have to cross a region is constant for a given period of time, and on the contrary, avoidance orders from the neighboring regions may increase this number. To illustrate the case, let consider the simple case of two neighboring regions that issue, at the same time, the same public avoidance level equal to 0.5. It means that 25% of the vehicles have to avoid both regions, 25% can enter both, and 50% have to avoid only one. Among the 50% that have to avoid only one region, there is one possibility that the new shortest-path in time always advises vehicles to cross the other region, which will offset the avoidance orders. In short, for each car that has to avoid a region, another coming from the neighbor will enter. In that particular case, only the vehicles that have to avoid both areas will not enter to one or the other, leading to an observed avoidance level equal to ${p^*}_i{}^t = 0.25$. This simple example illustrates the worst-case scenario when the observed avoidance level is only half the requested one. It is not a significant issue in practice as the feedback controller self-adapts to the perceived errors that result from the system reactions to the earlier control requests. The prize for a fully decentralized rerouting process is that the system may be less reactive as regional speeds converge slower to the reference. We will demonstrate in the sequel that the system performances are still excellent.

We will also investigate one extension of this framework to foster cooperation between the regions. To this end, we introduce a cyber-physical layer via a multi-agent system where each region is an agent characterized by its local spatial speed. This formulation aims to promote information transfers in a region vicinity to adjust avoidance levels considering the neighboring region states. This cyber-physical layer is created by physically connecting the regions via a specific policy, such

as minimum distance. Let consider a non-directed graph $\mathcal{G}(\mathcal{V},\mathcal{E})$ where each one of the nodes $i \in \mathcal{V}$ represents a single zone. A neighbor of the node i is a region j that shares a common border. In this case an edge $a_{i,j}$ declares the exchange of information between the two zones in a bidirectional way. The information that could be exchanged corresponds to the current regional states, like the regional speeds ${u_i}^t$ and ${u_j}^t$. However, as reference speeds may differ across regions, we prefer exchanging their normalized counterparts, i.e. ${r_i}^t$ and ${r_j}^t$, where ${r_i}^t = {u_i}^t / {u_i}^*$. We denote the set of all neighbors of i as $\mathcal{N}_i$.

Let consider the situation when multiple neighboring regions experience different congestion levels at the same time. Different avoidance levels result from the local proportional controller, which introduces competition between the regions when vehicles change their itineraries. If one region opts for strict entry restrictions, the neighbors will suffer from an increase in vehicle accumulation while trying to detour vehicles for themselves. A cooperative control framework can be inspired by the classical consensus algorithm (Olfati et al., 2007). The main objective is to enforce homogeneity between the neighboring regions, i.e., similar ${r_i}^t$ values. In the consensus case, specific results have been obtained when the graph $\mathcal{G}$ is fully connected, and all agents participate in the consensus protocol. In this case, the cooperative control law, labelled as Cop_1, is as follows:

$$(Cop_1): \quad p_i^t = \alpha\ K_p e_i^t - (1-\alpha) K_p \sum_{k\ \in\ \mathcal{N}_i} r_i^t - r_k^t \tag{2}$$

The objective of such a control law is to provide two sources of control combined via a convex combination. The first source considers local information only and corresponds to the previously stated proportional controller. The second term contributes to the cooperation setting. The main idea is to consider the differences between neighboring traffic states. When a region's speed is significantly lower than its neighbors, its avoidance level can be increased to release the local burden and improve homogeneity between regions. Contrarily, when the region's speed is superior, the region's situation is less critical compared to its neighborhood. The region's avoidance level can be reduced to help other regions in alleviating their congestion levels.

We also propose a second cooperative option Cop_2. The second term copies the local controller formulation considering now the average errors among all the neighbors, including the targeted region. The rationale is that the controller mixes its own decision with a decision taken at a larger scale, i.e., considering all neighboring regions.

$$(Cop_2): \quad p_i^t = \alpha\ K_p e_i^t - (1-\alpha) K_p \max\left(\frac{1}{n} \sum_{k\ \in\ \mathcal{N}_i + i} \left(u_k^* - u_k^t\right), 0\right) \tag{3}$$

Both former cooperative frameworks can be implemented in a centralized manner by using algebraic terms:

$$\begin{aligned} (Cop_1): &\quad \boldsymbol{p^t} = \alpha\ K_p \boldsymbol{e} \ -\ (1-\alpha) \boldsymbol{K_p}\ \boldsymbol{L}\ \boldsymbol{r} \\ (Cop_2): &\quad \boldsymbol{p^t} = \alpha\ K_p \boldsymbol{e} \ -\ (1-\alpha) \boldsymbol{K_p} \left(\max\left(\boldsymbol{A} + \boldsymbol{I}\right) \boldsymbol{D}^{-1}\ \boldsymbol{e},\ 0\right) \end{aligned} \tag{4}$$

Where $\boldsymbol{p}$, $\boldsymbol{e}$, $\boldsymbol{u}$, and $\boldsymbol{r}$ correspond to the vectors containing the control, errors, regional speeds, and normalized speeds for each region. The matrix $\boldsymbol{K_p}$ is a diagonal matrix containing the local proportional controllers; the matrices $\boldsymbol{A}$ and $\boldsymbol{D}$ are the adjacency and the degree matrices of graph $\mathcal{G}$ and $\boldsymbol{L}$ corresponds to the Laplacian, i.e. $\boldsymbol{L = A\text{-}D}$. The algebraic characteristic of the control makes it suitable for a centralized implementation in a traffic control center.

2.3. Reference speed estimation

The centralized controller requires a reference speed in each region. Like in perimeter control, we set this value to maximize the region outflow, which is equivalent to minimizing the total travel times. In practice, we need historical data to determine the Network Macroscopic Fundamental Diagram (NMFD) in each region and identify the critical density and speed. Those values are observed when the mean flow or travel production is maximum, also referred to as the capacity. Fig. 2 shows, as an example, data from two cities in Europe (Zurich and Lyon). The definition of the critical speed is quite straightforward as long as the network experiences oversaturated traffic states. (Ambhül et al., 2018) proposes an advanced method using re-sampling techniques to characterize the critical density even when oversaturated states are not frequently observed. It can be applied to learn and adjust the critical speed in practice. Note that NMFD usually exhibits a nearly flat region around the capacity, see Fig. 2a. Multiple critical speed values can then be related to capacity. In such a case, the lowest value should be favor as it corresponds to a density that minimizes the total travel time. This also means that the critical speed estimation does not require high accuracy, as errors in speeds close to the capacity have little impact on the outflow. Finally, note that NMFD can exhibit hysteresis loops with different shapes during network loading and unloading, see (Leclercq and Paipuri, 2019) for more details and a literature review. Fig. 2a slightly shows this kind of trend with lower capacity but higher critical speed during the unloading. In such a case, it is essential to adjust the reference speed for different periods to improve controller efficiency. Should a single value be used, the lower critical speed, the better to avoid early control triggering during the network loading at a suboptimal outflow regime, which would result in network inefficiency.

3. Case studies

All numerical experiments are run with a microscopic simulation platform as the plant model. It ensures realistic behavior for users travelling in the network and complete integration of the re-routing process we have described in

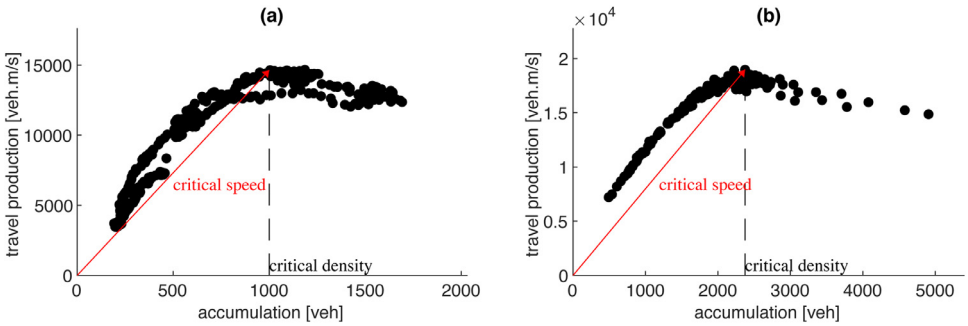

Fig. 2. Determining the critical speed (a) Zurich city (Wiedikon district), data courtesy of the transportation department at ETHZ; (b) Lyon city, (North), simulated data.

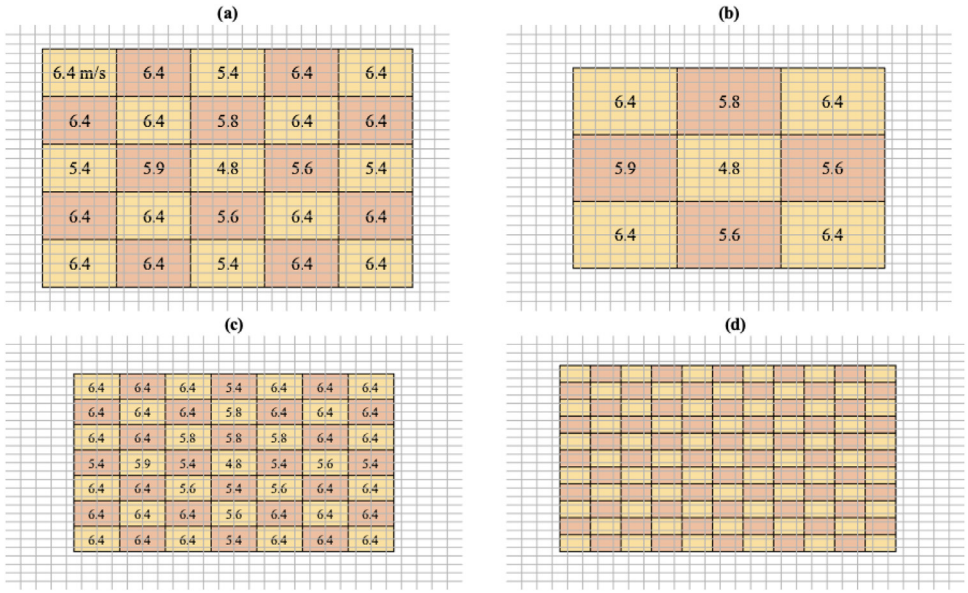

Fig. 3. Manhattan network (a) 5 × 5 partition – reference setting; (b) 3 × 3 partition; (c) 7 × 7 partition; (d) 11 × 11 partition.

Section 2.1. The simulations are performed using the Opensource microscopic dynamic tool Symuvia (https://github.com/lfsttar/Open-SymuVia). The car-following law is based on the Lagrangian resolution of the LWR model (Leclercq et al., 2007). This car-following law has been further extended to account for all features of urban traffic: bounded acceleration (Leclercq, 2007), lane-changing with relaxation (Laval and Leclercq, 2008), multiclass traffic, signalized and unsignalized intersections (Chevallier and Leclercq, 2009), roundabouts (Chevallier and Leclercq, 2008). A dynamic traffic assignment component has been recently integrated (Ameli et al., 2020a).

We consider here two case studies. The first one is a Manhattan (grid) network. We use it to perform detailed investigations on the concept and run all sensibility analysis. In addition to the control system's three primary parameters and the different control frameworks previously described, we will also study the impacts of the demand levels. The second test case corresponds to a real city network (northern part of Lyon, France) with a realistic demand pattern. It will complement the previous studies by assessing the system performance in a more elaborate setting.

3.1. Manhattan network

The road network is a 29 × 29 bidirectional squared grid, see Fig. 3. The distance between two intersections is 300 m. All intersections are signalized with a fixed-timing of 30 s red and green. The simulation time-step is equal to 1 s. The origins and destinations are the entry and exit links at the network border. So, we count 116 origins (O) and 116 destinations (D). The total demand profile varies with time to mimic the usual network loading and unloading during peak hours, see Fig. 3. The total demand is split uniformly among all entries. A single shortest path in distance is considered between all OD pairs as the regular path for users in the absence of control actions (uncontrolled case). The demand distribution between origins and destinations aims to reproduce a loading gradient from the network center to the edges, i.e., more vehicles drive in the middle than in the periphery.

Table 1
The different demand profiles.

Demand profile	D_1	D_2	D_3	D_4	P_1	P_2	P_3	P_4	# veh	Peak intensity
	[veh/s]				[min]				generated	vs. (R)
Profile A (R)	0.58	1.40	2.66	0.58	20	30	60	115	16,743	0%
Profile B	0.58	1.40	2.70	0.58	20	20	60	160	18,475	2.5%
Profile C	0.58	1.40	2.53	0.58	20	40	60	115	16,470	−2.5%
Profile D	0.58	1.40	2.40	0.58	20	30	60	85	15,426	−7.9%
Profile E	0.58	1.40	2.27	0.58	20	30	60	85	14,803	−14.4%

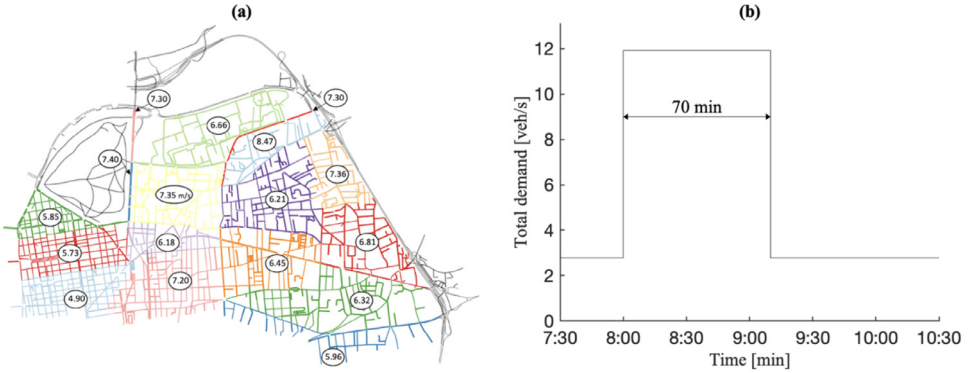

Fig. 4. Lyon 63 V network (a) road network, regions and reference speeds; (b) remand profile.

Five different demand profiles are considered, see Table 1. The first, profile A, defines the reference case where congestion is significant during the peak in the central network (the nine inner regions considering the 5 × 5 partitioning). Profile B increases the vehicles generated during the peak by 2.5%. It is close to the worst-case scenario as the network quickly goes to gridlock if we further increase the demand level. Profile B has a longer simulation duration as congestion needs more time to recover. Profile C to E, have less demand during the peak. In extreme case E, only minimal congestion is observed in the central network. These five scenarios provide contrasted network loading and permit to assess the controller performances in a wide range of congestion levels.

Four different partitions are considered to investigate different region sizes. Hence, 9 (3 × 3), 25 (5 × 5), 49 (7 × 7), and 121 (11 × 11) regions are used to cluster the full road network, see Fig. 3. The number of intersections included in one region is respectively 49, 25, 9, and 4. Note that network links close to the perimeter are never included in a controlled region and then never receive avoidance orders. It ensures that all vehicles have at least one viable option to go from their origins to destinations. The reference values for the safety distance d and the control horizon T are 600 m and 3 min. Other values will also be tested. Finally, the reference speeds have been adjusted, looking at the NMFD for the reference scenario and the 5 × 5 partition, see Fig. 3a. The reference speeds for other partitions have been tuned by considering the value set for 5 × 5 partition in the region with the most substantial overlap. Those values are presented in Fig. 3, except for the 11 × 11 case, as it would have been unreadable.

3.2. Real world network (Lyon 63V)

We will also test the new traffic control concept on a real network. To this end, we consider the northern part of Lyon Metropolis, see. Fig. 4a. This network has 1883 nodes, 3383 links, 94 origins, and 227 destinations. Origins and destinations are distributed along the network perimeter (main contact points with the other road networks) but also internally. Note that vehicles are always allowed to drive into the region where their trips start or end. All intersections are set with their existing characteristics during peak hours and, in particular, their regular signal timings. The simulation time step is equal to 1 s.

The demand pattern has been estimated based on travel surveys and vehicle counts at loop detectors inside the perimeter. It reproduces the typical loading and unloading congestion patterns observed during the morning peak hours from 7:30 to 10:30, see Fig. 4b. In total, 68,573 trips are generated during this period. The simulation is populated not only with car traffic but also trucks, buses, and tramways. Only cars react to the control scheme. The reference case is obtained by running a dynamic traffic assignment process that makes the network converge to user equilibrium (Ameli et al., 2020a, 2020b). This process includes a path discovery module based on shortest-paths in time. Around ten alternatives are considered for each OD pairs.

Fig. 4a shows how the network has been partitioned for control purposes. We did not use advanced clustering technics here, but we follow the following rational that resorts to our expert knowledge of the city. First, we decided not to include

more than two main arterials in a region and better keep this number to one. The idea is that we should let users enough flexibility to find alternatives when a region starts receiving avoidance orders. The whole area is crossed by four main arterials from West to East and about three from North to South. Second, we carefully checked that the critical nodes, i.e., the intersections that carry most traffic and are usually congested, do not belong to the same region. The reason is again to provide options for rerouting when a region is inaccessible for some users. Third, we carefully designed the clusters to prevent arterials from being on one region's side. This avoids the situation when a user can easily switch from an arterial to nearby roads in a neighboring region. Such changes may have little effect on the overall system performance as the roads are too close. Fourth, we ensured that an arterial crossing the full area belong to at least two regions. It creates possibilities to join the arterial again after avoiding it in an anterior region. Finally, we looked at the simulation results for the reference scenario to adjust the region boundaries. We tried here to ensure that traffic states during peak hours are relatively homogeneous. This last criterion is usually enforced for perimeter control applications, and we included it as our centralized controller has some similarities with such traffic management strategies. We end up with seventeen regions. Note that three of them are composed of a single arterial segment. Those segments are critical in the sense that the only alternative paths are close and cannot be aggregated in the same region. Again, the reference speeds are adjusted, looking at the NMFD for the reference scenario. The resulting values are displayed in Fig. 4a.

4. Results

This section presents the overall assessment of the new control concept. First, we start with the most straightforward reactive controller, i.e., the decentralized proportional feedback one, because it has a single parameter K_p and proves itself already very valuable. We provide a complete description of the system functioning from both the network and the vehicle's point of view for the reference demand profile A. Second, we perform a complete sensitivity analysis to determine the optimal settings for K_p and the safety distance, d. The influence of the congestion levels related to the different network loading is also investigated. Third, the control time horizon and the region size are investigated again on the Manhattan network to provide a full and comprehensive review of the system performances. Fourth, we test more advanced controller formulations including some levels of cooperation with the neighboring regions. Fifth, we consider the influence of the initial network loading for the Manhattan network. Finally, we conclude this section with more analysis concerning the real-world network case. Note that comparing our new control concept with existing perimeter control strategies is very challenging as (i) each single control strategy requires specific calibration, which is far from trivial, and (ii) multiple solutions have been proposed to implement perimeter controls in a multiregional setting. So, it is difficult to provide a benchmark that would be non-disputable. Annex 1 presents a first step in this direction by considering a simple reactive perimeter control strategy.

4.1. Controller performances for the Manhattan network, 5 × 5 partitioning, and the reference demand profile

We first run the proportional controller with $K_p = 0.5$, $d = 600$ m, and profile A. This setting is very close to the optimal one, see next Section 4.2. Fig. 5 presents the time-evolution of the mean speed in each region (5 × 5 partitioning) in the uncontrolled and controlled cases. Reference speeds in each region have been added in dashed lines to track the controller behavior better. We already mentioned, when presenting the Manhattan test case, that profile A leads to severe congestion in the central part of the grid network during the peak. Each of nine inner regions experiences speeds below critical during a large part of the simulation, and those values can go down below 2 m/s. The peak demand level is achieved between 50 and 110 min. A time-lag can be observed between the peak at the entries, and the congestion development inside the network. It is because the network is vast, about 9 km in width, and congestion needs time to propagate. In the same vein, after the demand drops, it takes more than 1 hour for the network to recover fully, which is a typical pattern during network unloading.

Let now focus on the control system impacts. While not always tightly tracking the reference speed in all regions, the controller has a significant positive impact. All nine inner regions have higher speeds that are most of the time close to the reference, except from time to time when the controller needs time to adapt. On the contrary, the peripherical regions experience lower speeds than in the uncontrolled case, but such speeds are always above critical, meaning that those regions never suffer from saturation. Fig. 5 highlights that the control system is acting as planned. The avoidance maps push the vehicles away from the congested regions (inner network) to the regions which can afford more vehicle traveling without deteriorating the travel production. The fact that the controller is sometimes slow to converge to the reference speed is not surprising as (i) we are indirectly implementing the control actions, and (ii) the control time horizon is set to 3 min. When a new avoidance map is generated, it does not imply that the region inflows immediately adjust to the new avoidance level p_i^t. It takes time for vehicles being redirected to other paths. Even if the changes in inflows would happen instantaneous, it would not trigger fast changes in speed, as congestion needs time to resorb when the demand drops. So, it is perfectly reasonable that the controller needs time to adjust the region's speeds and converges to the reference values. It should be noticed here that even if we use a basic and fully decentralized implementation of the system (individual proportional controllers in each region with no cooperation), the overall performances are excellent. The total travel time experienced by users at the network level is reduced by 15.5% over the total simulation. We define the total travel time improvement V_{ttt} as the positive value of the variation of the total travel times between the uncontrolled and the controlled cases.

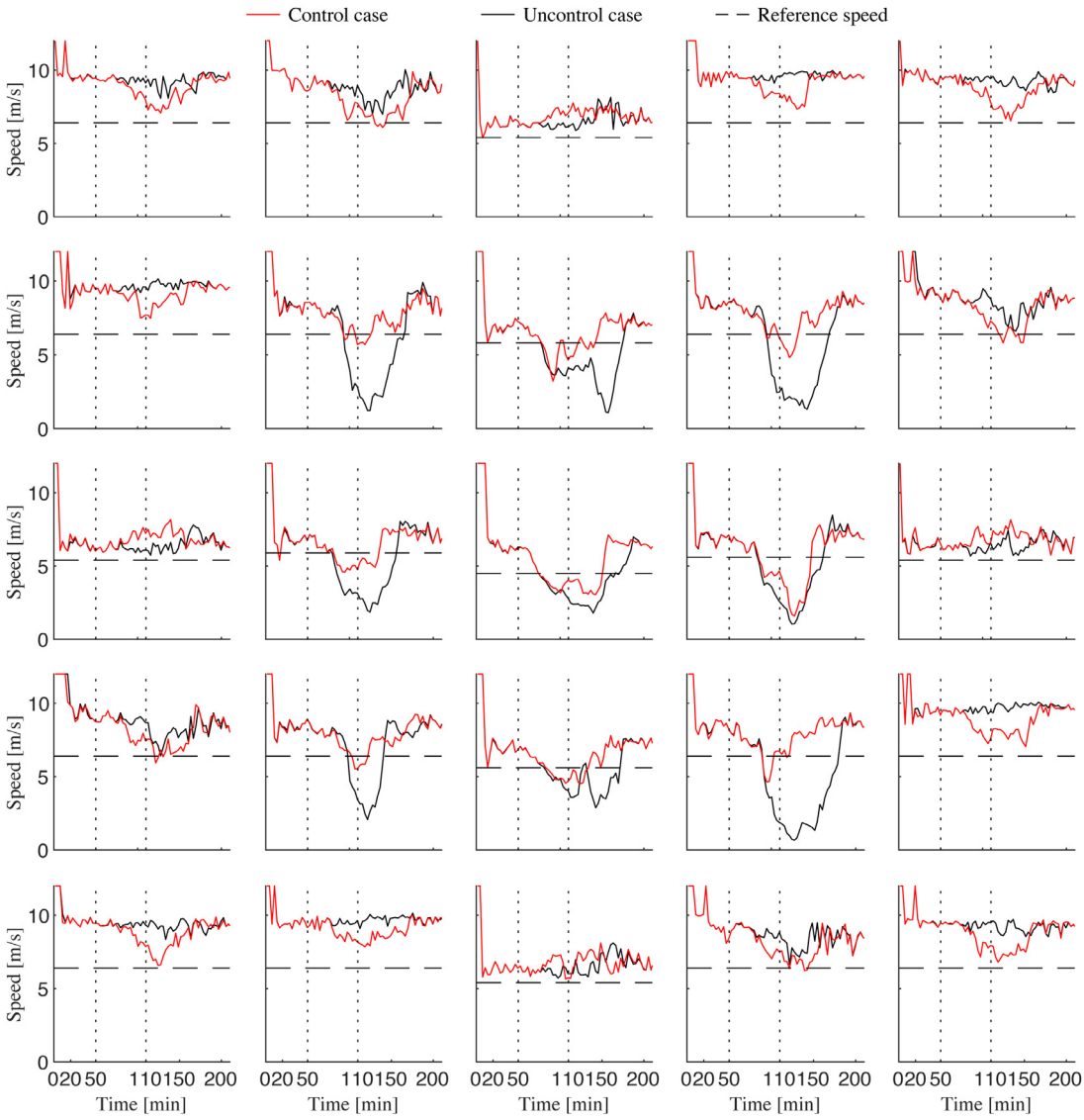

Fig. 5. Evolution of mean speed in the 5 × 5 regions for the reference scenario (Manhattan network).

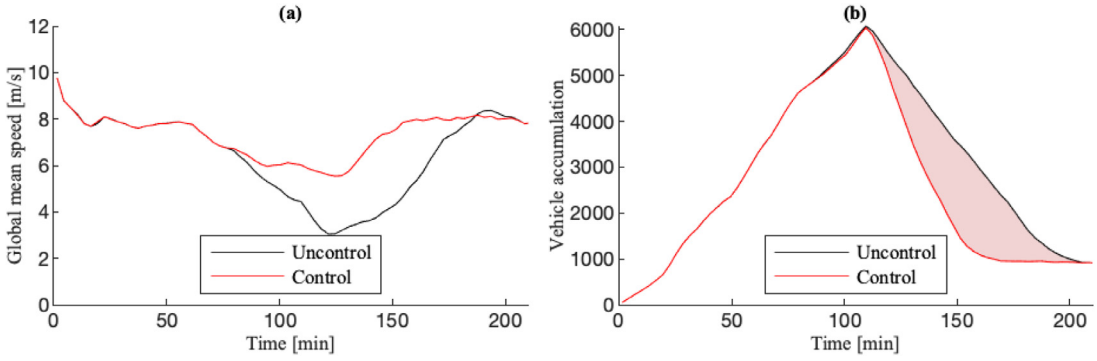

Fig. 6. Evolution of (a) the global mean speed and (b) the vehicle accumulation for the reference scenario (Manhattan network).

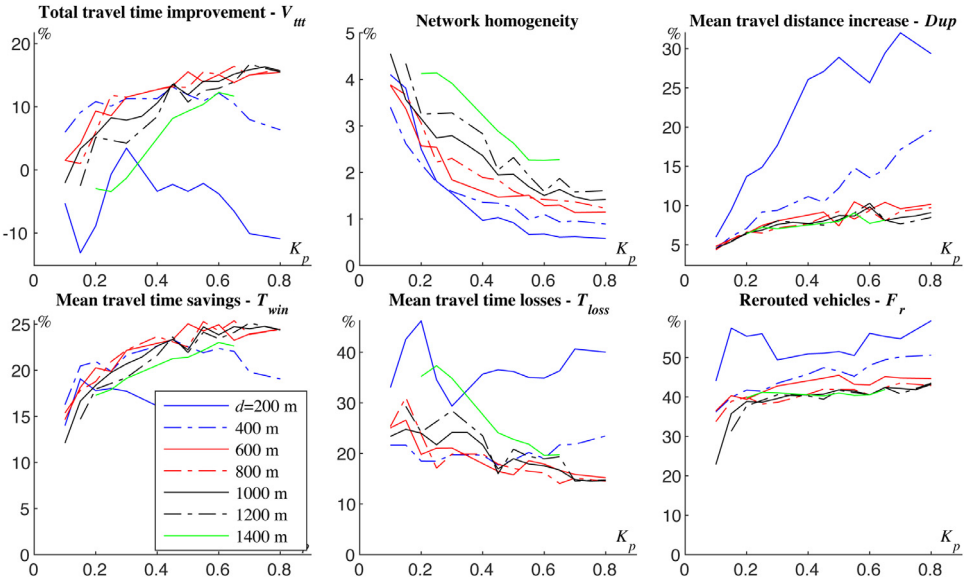

Fig. 7. Sensibility analysis to K_p and d for profile A (Manhattan network).

Fig. 6 presents more evidence about the system functioning at the network level. Most of the total travel time gains are achieved during the network unloading, as shown in Fig. 6b, when looking at the difference in vehicle accumulation between the control and uncontrol cases. Let recall here that the area below the time-evolution of the accumulation over the simulation corresponds to the total travel times spent by all vehicles in the network. This improvement comes from the network state achieved with the control at the end of the loading phase. As the speed is much higher at time $t = 110$ min with the controller active, in particular in the central region, the congestion recovering is much faster. The mean network speed over the simulation increases from 4.91 m/s to 6.76 m/s. Furthermore, the speed homogeneity among regions is much better with the controller. The variance of the mean speed between the 25 regions drops from 4.91 to 1.49 by the controller actions. By rerouting vehicles, the controller improves their distribution over the network and leads to less congestion and faster network recovery. We should now investigate the individual impacts on users to ensure that the cost for optimality at the network level is not too high for individuals.

We define a bunch of indicators to understand the controller behavior better at the vehicular level:

- F_r [%]: the fraction of vehicles that received at least one rerouting advise during the simulation as their regular path would have crossed a restricted region;
- F_d [%]: the fraction of vehicles that experience an increase in travel distance compared to their original path;
- D_{up} [%]: the mean travel distance increase considering only vehicles with an increase higher than 2%;
- F_t [%]: the fraction of vehicles that experience a travel time increase compared to the uncontrolled case;
- T_{win} [%]: the mean individual travel time reduction considering only vehicles with lower travel times in the control case;
- T_{loss} [%]: the mean individual travel time increase considering only vehicles with higher travel times in the control case.

For the reference scenario and the current controller settings, we get $F_r = 45\%$, $F_d = 37\%$, and $D_{up} = 7.4\%$. As the congestion is important in the uncontrolled case, the controller needs to change paths for about half the vehicles. However, 53% of the vehicles see no changes in their travel distance, and the mean increase for the others is rather limited. Only 5% of the vehicles see their distance increased by more than 20%. So, the individual impacts look rather acceptable when compared to the collective gains at the network level. The other indicator values are $F_t = 26\%$, $T_{win} = 25\%$ and $T_{loss} = 15\%$. As the network conditions improve, it is not surprising that most vehicles experience travel time gains. Still, 26% of the vehicles have higher travel time. The mean increase (15%) seems reasonable compared to the mean reduction (25%) offered to the vast majority. We can conclude for this scenario that even when using a straightforward non-predictive and non-cooperative controller formulation, we observe significant improvement at the network level with reasonable individual impacts.

4.2. Sensibility analysis to the controller parameters and the demand patterns for the Manhattan network

We first present a thorough sensitivity analysis to the controller parameters (K_p and d) for the reference demand level. Fig. 7 shows all results for the primary indicators at the network and individual levels. We add the tracking of the network homogeneity defined as the variance of the regional mean speeds over the simulation.

The first conclusion is that small safety distance, i.e., $d = 200$ and 400 m, harms the system efficiency in all ways. For $d = 200$ m, the variation of the total travel time compared to the uncontrolled case is positive for almost all K_p values.

Table 2
Optimal controller parameters for the different demand profiles (sorted by descending order).

Demand profile	K_p	d
Profile B	0.65	600 m
Profile A (R)	0.65	800 m
Profile C	0.65	800 m
Profile D	0.7	1200 m
Profile E	0.7	1200 m

The network performances are, therefore, worse than without control. When $d = 400$ m, the control improves the network conditions but significantly less than with higher distance values. Note that those two distance values also lead to poor results at the vehicular level. The mean travel distance increase due to the control is very high, as well as the mean travel time losses. Let recall the fundamental role played by this parameter. When a vehicle is closer than d from an inaccessible region, it ignores the avoidance order. On the one hand, small safety distance means than more vehicle will react to a newly pushed public avoidance maps as the number of disregarded orders will be small. On the other hand, it also means that vehicles will have to reroute on short notice and very close to a region perimeter. It generates higher distance traveled as vehicles cannot anticipate and find upwind an alternative that does not involve a substantial increase in travel distance. This effect can be seen in both the fraction of rerouted vehicles and the mean travel distance increase when $d = 200$ or 400 m. The former value is the worst-case scenario as the network link length is 300 m. All these changes of directions on short notice certainly create new congestion into the network leading to overall lousy efficiency.

The best system performances are observed when the safety distance is between 600 m to 1200 m. Note that 600 m means in the Manhattan network that vehicles are at least two intersections ahead of the next crossed region, which looks reasonable to find a new alternative path in case this region is inaccessible. When the distance is very high, $d = 1400$ m, the system does not reroute many vehicles or leads to significant travel distance increases, but it does not function well either at the network level. It is undoubtedly because too many vehicles can disregard the avoidance orders, which makes the system less reactive in releasing the burden of the congested regions.

So, the safety distance appears as a critical parameter to calibrate. Fortunately, the range of values associated with high levels of performance is broad, from 600 to 1200 m, so the system should be robust to medium scale calibration errors for this parameter. We will discuss in the sequel how it is sensitive to the region sizes. We now focus on the influence of the proportional controller parameter K_p. All results point out in the same direction: the higher K_p values (in the reasonable range between 0.2 and 0.8), the more traffic conditions improve. For demand profile A, the total travel time reduction can go up to 16.7%. High K_p values also improve travel time savings and minor mean travel time losses. On the other hand, high K_p values induce more rerouted vehicles, and higher travel distance increases. So, the system appears to act that way: higher K_p values make the controller more reactive to a given difference in the actual speed vs. the reference. In other words, it requests a higher avoidance level for the same errors, which lead to more vehicle rerouting. It has a positive effect at the network level, but it comes at a high cost for individuals in terms of travel distances. So, to optimally tune the controller, it seems essential to balance those effects and to build an objective function that considers both the network and the individual scales. The mean travel time savings and losses follow a similar trend as the total travel time improvement. Likewise, the fraction of rerouted vehicles seems correlated to the mean distance increase. We propose then to focus only on two independent criteria to define the objective function: the total travel time improvement (V_{ttt}) and the mean individual distance increase (D_{up}). We weighted these two criteria equally after normalization. The resulting optimal controller setting is $K_p = 0.65$ and $d = 800$ m. In Fig. 7, V_{ttt} and D_{up} curves look nearly flat in a range of K_p values between 0.55 and 0.8. It is remarkable as it means that the controller is not very sensitive to K_p around the optimal value, which makes it robust to medium scale calibration error.

Table 2 presents the optimal parameter setting for all demand scenarios from A to E. It appears that when the demand level increases, the optimal K_p values tend to decrease slightly from 0.7 to 0.65 as well as the safety distance d. The decrease in d is much pronounced as it moves from 1200 m to 600 m. When the congestion level is low (Profile D and E), it does not matter if vehicles are finally authorized to enter the next unavailable region even if they are still quite far (1200 m). Such a setting smooths the rerouting operations and indeed leads to lower increases in travel distance. When the congestion becomes severe (Profile A and B), stricter avoidance rule should be enforced, and vehicles have to reroute even when the next crossed region is close (600 m). We also compute the overall optimal setting, which minimizes the objective function across all scenarios. The results are $K_p = 0.7$ and $d = 1200$ m. It means that if we look for a global setting that works for a broad range of demand profiles, it is better to opt for a higher safety distance.

Considering the optimal setting for all demand levels, we can further investigate the system performances. Fig. 8a shows the total travel time improvement and the mean network speed with and without control for the five demand profiles. The system performs very well for all demand levels, as the mean network speed is high and stable when the control is active. On the contrary, it significantly decreases for higher demand levels otherwise. So, the total travel time improvement increases with the demand level from 1.59% to 30.6%. Fig. 8b better explains what happens at the network level. When

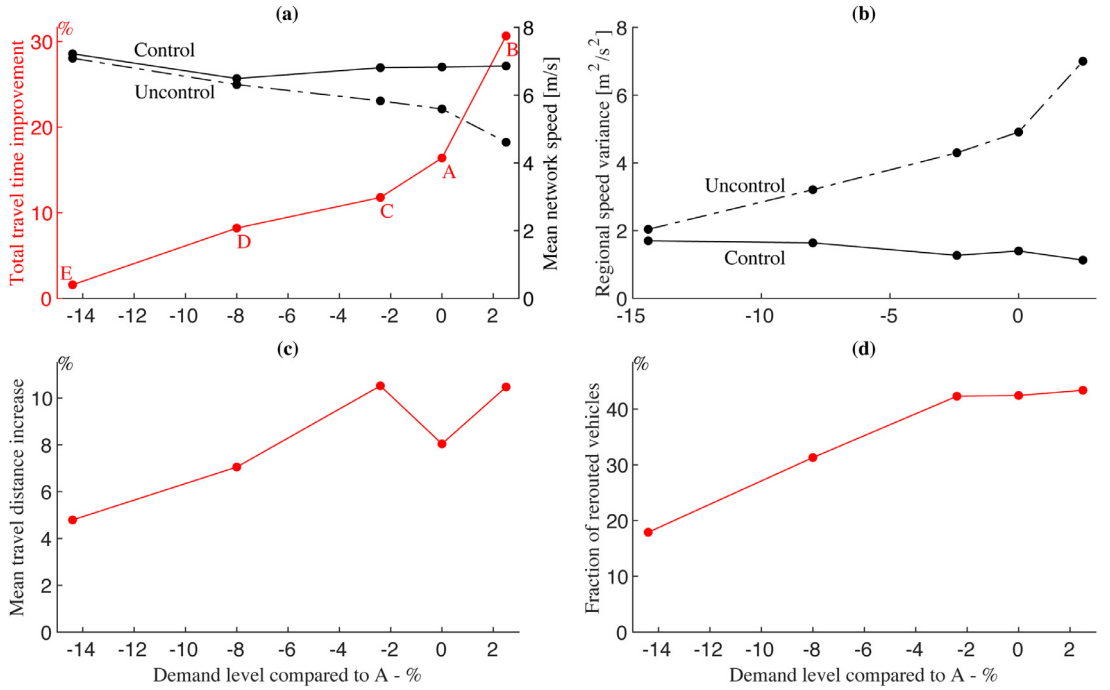

Fig. 8. Influence of the demand level on the controller performances (Manhattan network). (a) total travel time improvement (V_{ttt}); (b) network speed homogeneity; (c) mean travel distance increases for rerouted vehicles (D_{up}); (d) fraction of rerouted vehicles (F_r).

the network heterogeneity (variance of the regional mean speeds) increases from 2 with profile E (lowest demand) up to 7 with profile B (highest demand) without control, it remains small and stable around 1.5 when the avoidance system is active. We have thus demonstrated that the centralized controller properly sets the public avoidance map, and induces adequate vehicle re-routings. It is a convincing proof that the concept can be useful in the real world. Fig. 8c and Fig. 8d provide further details at the individual level. When the demand increases, the mean travel distance by rerouted users also increases. It was expected as the system issues more avoidance orders to protect some regions from heavy congestions. What is important here is that the mean travel distance increase remains reasonable even when the demand is very high (profile B). The highest D_{up} value (profile B) is not higher than 10.5%, while it remains below 5% for the lowest demand levels. Finally, Fig. 8d shows that system activity increases with the demand level. The fraction of rerouted vehicles is equal to 17.9% for profile E and reaches 43.4% for profile B. It should be noticed that while the number of vehicles that is impacted by the system increase by 2.5 times, the mean travel distance increase remains reasonable. This result is crucial to transfer the system into practice as it means than the requested individual efforts are more likely to be accepted.

To conclude this sensitivity analysis, let us mention that we have extensively tested more advanced controller formulations by adding integral and derivative terms to match with the complete and classical PID framework. However, none of these additions provide improvements compared to a simple proportional feedback. Adding an integral term even significantly worsens the controller performance. Our interpretation is that the system is not very reactive because of the substantial time lag between the moment when the avoidance map is pushed and when the avoidance levels are fulfilled by all vehicles for a given region. So, the integral term tends to stress past errors too much. As those errors result from the slow system adaptation, it should better adjust straight away to the current observed speed gaps. The derivative term does not substantially harm the controller performances. However, it does not improve them either, so we preferred to keep the controller formulation minimal and reduce the number of parameters. Up to now, all regions have their controller selfishly acting based on the local observations. We will investigate in the sequel more advanced formulations, which introduce cooperation between neighboring areas.

4.3. Controller performances under different time horizons for the Manhattan network

In this section, we investigate the influence of the control time horizon T, i.e., the frequency when the public avoidance map is updated. We restrict the analysis to three demand profiles (A, B, D) and the two primary assessment criteria: the total travel time improvement (V_{ttt}) and the mean distance increase (D_{up}). We did not carry the computational burden of calibrating the controller parameters K_p and d for new T values again. So, the results for $T \neq 3$ min may not be optimal, but we can still analyze the overall trends.

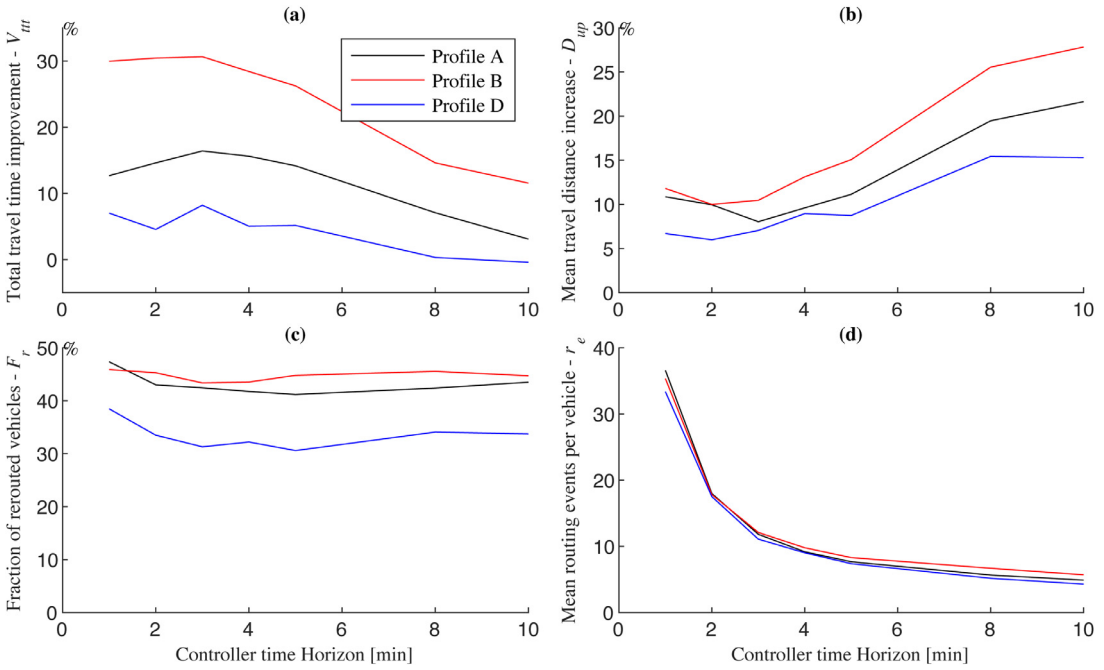

Fig. 9. Influence of the controller time horizon T (Manhattan network). (a) total travel time improvements; (b) mean travel distance increases for rerouted vehicles; (c) fraction of rerouted vehicles; (d) mean routing events per vehicle.

Fig. 9a presents the variation of V_{ttt} with respect to T. It appears that the system performances are high until $T = 3$ min and then decreases when T increases. The overall performances fall from 12% to 3% for profile A, from 30% to 11% for profile B, and from 8% to almost 0% for profile C. Fig. 9b shows that the mean travel distance D_{up} follows the exact opposite trend: the mean travel distance even triple in the worst-case scenario (profile B). There is no surprise that when the control time horizon is too high, the control system is not reactive enough to alleviate the congestion. On the one hand, the avoidance levels are not updated frequently enough to account for the system reactions to the control. It is one well-known drawback of the proportional control framework, which includes no prediction and requires frequent updates from the system. On the other hand, inappropriate avoidance levels force vehicles to significant detours, which explain the significant increase of the mean individual travel distance. We can conclude here that control time horizons broader than 3 min are not appropriate.

To further investigate the optimal control time horizon setting, we look at two more criteria. Fig. 9c shows the fraction of rerouted vehicles F_r, which does not look very sensitive to the control time horizon, even if we see a slight increase when T values are small. Fig. 9d presents the mean number of routing events per vehicle r_e. It highlights the real impacts of low T values: as new public avoidance maps are pushed more frequently, vehicles have to calculate new routes at a higher pace. This number almost triple when T drops from 3 to 1 min. So, it is certainly not relevant for the system acceptability at the individual level to set up T to low values, even if the route calculations are done automatically by the navigation system. This short analysis shows that $T = 3$ min looks the best comprise for this network, and this is why we are using it from the beginning.

4.4. Controller performances for different region sizes and the Manhattan network

In this section, we investigate the influence of region sizes and consider the three other partitions: 3×3, 7×7, and 11×11, with a control time horizon set back to 3 min. We run the same optimization process as in Section 4.2 to determine the optimal controller settings (K_p and d) for all grids and three demand levels (A, B, and D). Let recall that the objective function balances the total travel time reduction ($-V_{ttt}$) and the mean individual distance increase (D_{up}). Fig. 10 presents the controller performances for all configurations and optimal settings. In addition to V_{ttt} and D_{up}, spider plots show the following simulation outputs: the fraction of rerouted vehicles (F_r), the mean routing events (r_e), and the mean travel time loss by vehicles that have been penalized by the control (T_{loss}). Travel time gains (T_{win}) have been omitted in the figures as they follow the same trend as V_{ttt}. All the displayed indicators should be minimized for better performance both at the network or the individual levels. So, the closer to the center the cobweb is, the better the controller acts.

Fig. 10 shows that the 3×3 partition always performs better than other region sizes for all criteria except V_{ttt} for profile B and D_{up} for profile D. When comparing together the other three partitions, it appears that the smaller the regions, the higher the network performance and the lower the penalties to users (D_{up}, r_e, and T_{loss}). Only F_r suffers an increase when the region sizes decrease. The ranking between the 5×5, 7×7, and 11×11 regional settings looks natural. With

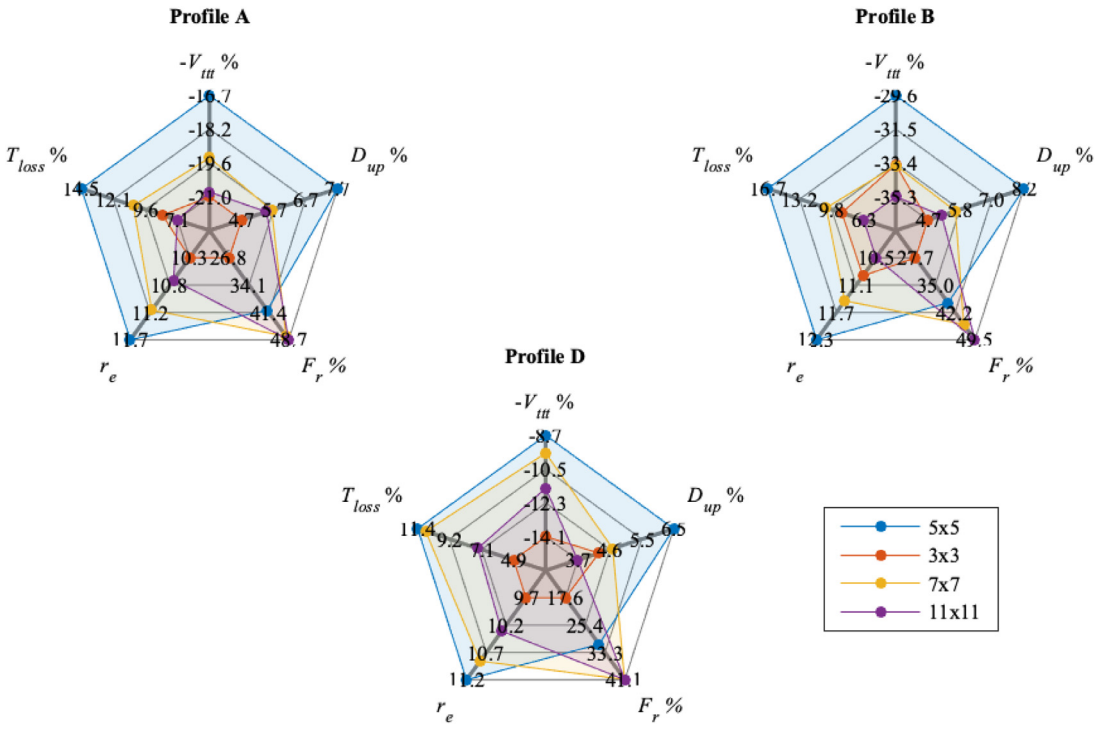

Fig. 10. Influence of the region sizes for different demand profiles (Manhattan network); V_{ttt}: total travel time reduction; D_{up}: mean individual travel distance increase; F_r: Fraction of rerouted vehicles; r_e: mean number of route events; T_{loss}: mean individual travel time loss.

more regions of smaller sizes, the controller can efficiently distribute the vehicle optimally across the network. Furthermore, avoiding smaller regions lead to lower detour, which improves D_{up}. However, more regions make it more likely for a vehicle to experience a detour, which explains the increase of F_r. The excellent results concerning the 3 × 3 partition are more tricky to interpret, and we should admit we do not have complete explanations. Our intuition is that, as the congestion starts from the center in this particular network, the 3 × 3 grid matches better the congestion spreading and leads to those excellent results. Thus, we consider this particular observation as too specific at this stage, to make any general statements about high region sizes.

It is difficult to draw general conclusions about the optimal region sizes, and further sensitivity analysis would be necessary considering different network configurations. What looks promising here is that no partition leads to unacceptable controller performances. If the controller functioning can improve with a better partitioning, which certainly means either considering more regions or region shapes that closely match the city congestion patterns, it can perform well with any partitioning. The variations across the different criteria are neither negligible nor huge when the region size changes. Another important conclusion is that the safety distance tends to increase with the region size when looking at the optimal parameter values. For example, $d = 400$ m for the 3 × 3 grid and demand profile A and increases to 1200 m for the 7 × 7 and 11 × 11 grids. With smaller regions size, it harms less the system to let a vehicle enters a next inaccessible region to prevent unnecessary detours. So, the detours are further anticipated, which leads to smaller D_{up} values in the end.

4.5. Introducing cooperation in the controller framework - Manhattan network

We now present the results for the two cooperative control frameworks we have introduced in Section 2.2 (Cop_1 and Cop_2). Both correspond to a convex combination of the individual proportional controller and a second term that considers information coming from the neighboring regions, see eq. (2) and (3). We did extensive tests with all demand levels, and it appears that the cooperative frameworks provide benefits only when the congestion is severe (profile B). We design these schemes to facilitate arbitrations between regions that experience severe congestion levels at the same time. Only situations where congestion spreads all over the network can improve through regional state information exchanges. We then restrict the analysis to profile B in this section.

Fig. 11a presents the control performances for different α values, representing the weight on the individual controller (first term) in the control law. When $\alpha = 1$, the control law reduces to the individual proportional controller (P). The lower the α value, the more weight on the second (cooperative) term. The bottom of the graph shows the evolution of the mean travel distance increase (D_{up}) while the top shows the reduction of the total travel times ($-V_{ttt}$) when the control is active. In between, we draw a line for each cooperative controller to show the overall objective function's variation compared to the

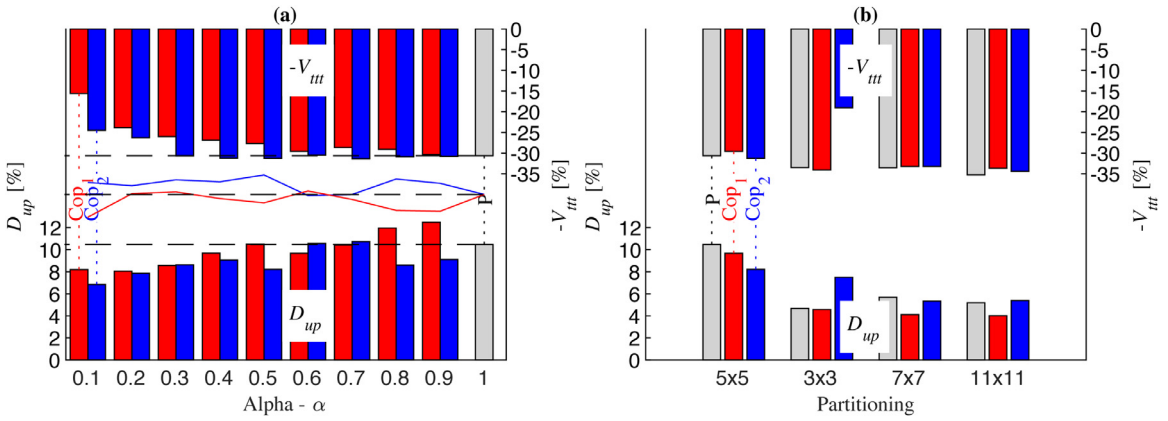

Fig. 11. Impacts of cooperation in the controller performances. (a) Total travel time improvements; (b) Mean travel distance increases for rerouted vehicles; (c) Fraction of rerouted vehicles; (d) Mean routing events per vehicle.

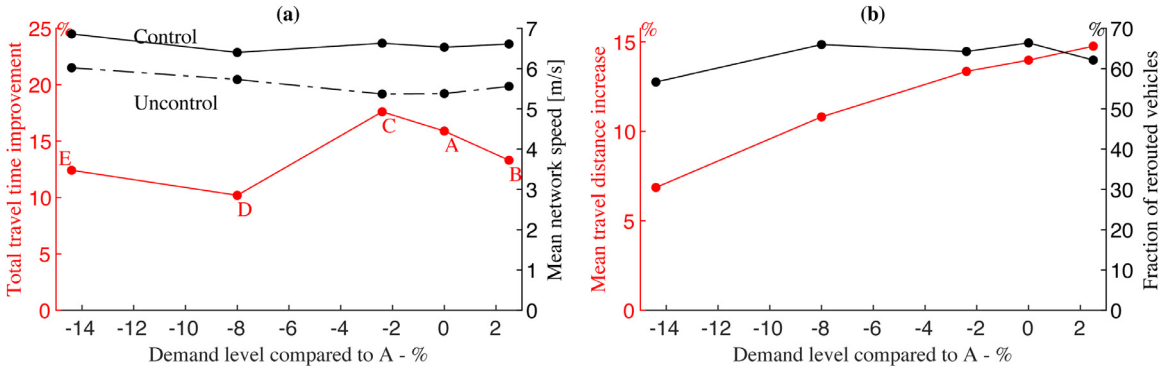

Fig. 12. Influence of the initial network loading (Manhattan network). (a) total travel time improvement (V_{ttt}); (b) mean travel distance increases for rerouted vehicles (D_{up}) and fraction of rerouted vehicles (F_r).

proportional controller only. Let recall that this objective function equally mixes D_{up} and -V_{ttt}. When those lines are above the black dashed horizontal line, it means that the cooperative controller improves the overall system performances. The main conclusion is that introducing a dose of cooperation tends to improve the system performances mainly by reducing D_{up}. The improvements related to Cop_1 are somewhat limited even when the maximal value is reached at $\alpha = 0.6$. When $\alpha \leq 0.4$, the total travel time reduction drops (from −30% for P to nearly −25%), but the mean travel distance increase is also significantly reduced, leading on average to overall stationary performances. This property can be interesting for operators if they choose to weigh more personal inconveniences than network performances. The results for Cop_2 appear much better. When $\alpha \leq 0.5$, the overall objective function is improved compared to the individual controller only. The optimal value is observed when $\alpha = 0.5$. It is interesting to notice that as long as $\alpha \geq 0.3$, Cop_2 sustains the same level of performance at the network level than the individual controller (same -V_{ttt} values) but shows better score at the individual level (lower D_{up} values).

Fig. 11a shows how cooperative frameworks behave when the region sizes change. The displayed simulation results correspond to the optimal controller settings, K_p, d and α. Optimal α values are determined based on sensitivity analysis: (0.6, 0.6, 0.2, 0.2) - Cop_1, (0.5, 0.5, 0.3, 0.6) - Cop_2 for (5 × 5,3 × 3,7 × 7,11 × 11) grids. The cooperative scheme results are not convincing for the 3 × 3 grid. It was expected as only the central region has a full set of neighbors in this configuration. The 7 × 7 and 11 × 11 grid results show that Cop_2 is not improving the situation compared to the individual controller. One explanation is that we only consider the immediate neighbors for each region. It reduces the overall spatial extend of the scaling-up process (Cop_2 considers the average error in the neighborhood) and limits the benefits from cooperation. On the opposite, Cop_1 provides more benefits as it sustains the overall network performances while reducing the D_{up} significantly. The smoothing process incorporated in Cop_1 that tends to make neighbors more homogenous looks more effective when more regions are into play.

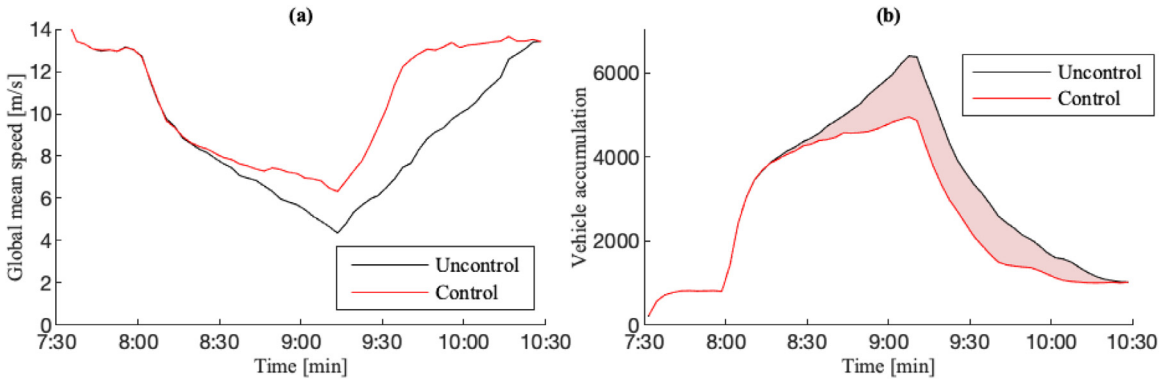

Fig. 13. Evolution of (a) the global mean speed and (b) the vehicle accumulation for the reference scenario (Lyon63V network).

4.6. Influence of the initial network loading – Manhattan network

In Section 3.1, we mentioned that the initial network loading (without control) in the Manhattan network assigns all vehicles to the shortest path in distance between their origins and destinations. When the congestion levels are high, some cars may look for new itineraries even when no control strategy is applied. This process is known as user equilibrium (UE) when all drivers try to minimize their travel times (Wardrop, 1952). To assess the sensitivity of the P-controller's performances to the initial network loading, we now start from an initial dynamic network loading corresponding to the UE conditions. It is calculated using simulation-based numerical methods (Ameli et al., 2020a).

Fig. 12 presents the impacts of the P-controller for the different demand profiles. The total travel time improvements (V_{ttt}) fall within the same range of what we observed with the previous initial network loading, with the notable exception of scenario B, i.e., the highest demand level. In that case, V_{ttt} is cut by two compared to the results shown in Fig. 8a but is still equal to 13.5%. When the demand level is high, a path assignment based on the shortest distance induces more massive congestion on the most crowded paths because users do not look for alternatives. The controller can then improve the total travel time by about 30%. Starting from UE conditions is more realistic for such a demand profile as it already includes user self-routing decisions related to the congestion. In practice, not all users are optimizing their trips, so while 30% can be seen as a rather optimistic upper bound for the controller performance for scenario B, 13.5% is undoubtedly the pessimistic one. Fig. 12a also shows that the controller improves the mean network speed for all demand scenarios.

Fig. 12b shows the evolution of the mean travel distance increase (D_{up}) and the fraction of the rerouted users (F_r) for all demand scenarios. When compared to the previous initial network loading in Fig. 8c and Fig. 8d, we observe the same trends. The D_{up} and F_r values are slightly higher when the UE is considered as the initial condition. The controller has to move more vehicles from their original paths and ask users for higher detours. As the initial condition is close to UE moving the effort to a system optimum state requires more actions at the individual scale. However, D_{up} values remain acceptable for all demand scenarios, around 14%, confirming relevance of the new proposed concept.

4.7. Final assessment for a real network

This last subsection discusses the application of the control concept on a real network, see Section 3.2 for the description. This network corresponds to the Northern part of Lyon city and has 17 regions. The reference scenario mimics the normal traffic states observed during peak hours. The individual proportional control is applied considering K_p=0.65 and d = 800 m. The speed and accumulation evolution are shown in Fig. 13. The overall travel time improvement (V_{ttt}) is significant and equal to 17.1%. This result falls the range of what we observed in the Manhattan network for heavy traffic conditions. This improvement is achieved through a lower speed variance (higher homogeneity) among regions when comparing the control (3.93) to the uncontrol cases (6.22). It shows that we can replicate the system good performances with more complex network topology corresponding to a real network and a realistic demand profile.

At the individual level, the impacts of the control are the following: F_r = 18.7%, D_{up} = 3.0%, T_{win} = 19% and T_{loss} = 15.4%. They are rather limited, as only 20% of the vehicles are rerouted with marginal travel distance increase on average. Only 5% of the rerouted users see travel distance increase higher than 22.2%, which looks moderate. The travel time increase for vehicles that do not individually benefit from the system is around 15%, which again seems reasonable. In summary, the controller performs very well on this new network with significant network gains and low individual impacts. Such results would require further confirmation for other demand loadings However, they represent a strong initial proof that the control concept is working fine when all vehicles are respectful to the avoidance guidance.

5. Conclusions and perspectives

This paper introduced a new concept for large-scale urban traffic control. The system includes a centralized controller that defines avoidance levels for different urban regions and decentralized routing decisions by vehicles. We demonstrated that such a system significantly reduces the total travel time spent by all vehicles, up to 30% (shortest-path in distance initial loading) or 17.6% (UE initial loading) in the Manhattan network and around 17% in the Lyon63V network and a realistic demand pattern. Those results are in line with previous studies trying to quantify the benefits from operating urban networks at system optimum rather than user equilibrium. By adjusting vehicles' itineraries, the system loads the network more homogeneously, making the congestion vanishing faster during the unloading phase. It may result in negative impacts at the individual level, like travel distance or time increases. We showed that such impacts are limited to reasonable values when considering the number of impacted vehicles, and the mean travel distance increases.

We presented in the paper a thorough sensitivity analysis of the critical system parameters. First, we showed that the optimal safety distance is in the range of 600 to 1200 m. Shorter distances create extra congestion pockets due to abrupt rerouting decisions from users. Higher distances make the system unresponsive mainly because delays are too long before avoidance levels are achieved. We also highlighted that the lower bound is more appropriate when the demand levels are high, or the region sizes are large. On the opposite, higher safety distances are suitable when the congestion is less severe, or the region sizes are small. When the system needs to be more reactive because either the routing options are low (few regions with large sizes) or the congestion is propagating fast (high demand level), it is better to reduce d values. Let recall that all vehicles that are closer to the next region than d can enter whatever the avoidance level is. When d is high, rerouting decisions cannot happen close to a region perimeter and fewer vehicles immediately adjust when its avoidance level is updated. Second, we found that 3 min is undoubtedly the optimal setting for the control time horizon. Lower values make vehicles adjust their itinerary too often while higher values significantly harm the system efficiency at the network level as the control updates are not frequent enough. Third, we showed that region sizes influence the system performances. While the system results in good performances, whatever the grid sizes are, the 3×3 and 11×11 settings outperform the other configurations in the Manhattan network for all demand levels. Our interpretation is that the 3×3 regions fit very well with the centric congestion distribution of this scenario. The 11×11 configuration looks the more impressive as smaller regions provide more flexibility for rerouting, leading to significant reductions of the mean travel distance increase across all region sizes. Small region sizes should be favored in the general case as they can more easily accommodate different congestion spreading patterns.

The optimal control proportional factor K_p depends on both the demand level and the region size. The second factor is not an issue as partitioning is usually defined once for all and is not supposed to change in real-time. The dependency on the demand level may be more problematic as it means that this parameter should be recalibrated when the demand patterns evolve. Fortunately, the system performances both at the network and individual levels are not very sensitive to the K_p values close to the optimum (flat objective function). So, a given K_p setting is robust, to some extent, to changes in demand levels. An adaptative learning process, e.g. (Jian-Xin et al., 2008), can also be incorporated into the control framework to adjust K_p, considering historical information about traffic states in the different regions.

While this paper is a first and convincing proof that the new control system is promising, many questions remain before early field implementations. First, we could not derive an overall mathematical framework, fully describing the new concept effects, but mainly resorted to simulation studies. Even if we performed extensive sensitivity analysis and considered two different network configurations, it would be essential to confirm our findings considering more general network configurations. Second, the new concept would undoubtedly benefit from applying more advanced control frameworks and embedding predictions in the centralized controller. However, the most pressing question is investigating the system performance when the penetration and compliance rates are not equal to one. We have to determine the minimal fraction of vehicles equipped with compatible navigation systems that still guarantee high-performance levels. We should also consider non-compliant users or make compliance related to the individual efforts, e.g., the travel distance or time increase, requested when itineraries are updated. It would make the system assessment closer to real-life situations. We are confident that penetration and compliance rates can have significantly lower values while the system still operates fine. It would be consistent with the Pareto principle, which states that 20% of the causes explain 80% of the consequences. In our case, a sufficient fraction of compliant users could improve the network states even if others stick to their original routes. We should then verify that compliers do not face tremendous effort compared to others.

Finally, the control system can be further extended to account for priorities among users. In such a case, it is essential to enforce a full compliance rate through appropriate regulations. Otherwise, it would be too easy for users to bypass the priority scheme. However, instead of randomly applying the avoidance levels to all vehicles, we can introduce exceptions for specific users, like car-sharers, emergency vehicles, public transportation, electric vehicles, and permit holders. It provides a flexible way of differentiating the network users based on their overall contributions to collective objectives and reward them through a more direct access to their destinations.

Annex 1 – Comparison with classical perimeter control strategies – Manhattan network

Here, we compare the new controller's performances with a classical perimeter control strategy for the Manhattan network. Setting up such a benchmark is tricky as the literature about perimeter control is vast, and multiple advanced formu-

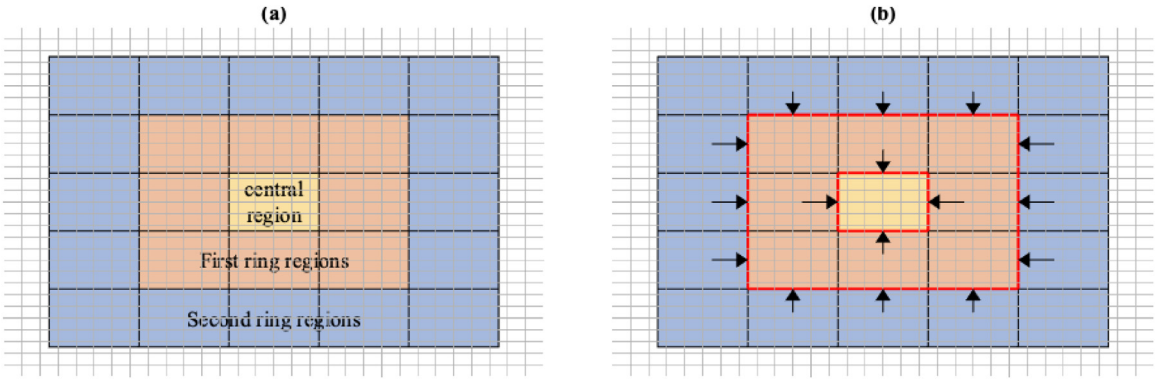

Fig. 14. Perimeter control monitoring and implementation. (a) ring definition (b) centric-implementation.

Table 3
New concept vs. perimeter control strategy – Manhattan network and scenario A.

	New concept		Ind. perimeter control		Centric perimeter control	
	Initial loading	UE loading	Initial loading	UE loading	Initial loading	UE loading
Travel time improvement (V_{ttt}) -%	16.4	15.9	2.5	0.6	1.4	0.5
Mean travel distance increase (D_{up}) -%	8.1	13.9	0	0	0	0
Vehicle with reduced travel time (F_t) -%	74	72	61	54	55	51
Mean individual travel time reduction (T_{win}) -%	25.4	21	10.2	4.2	11	4.4
Mean individual travel time increase (T_{loss}) -%	14.1	13.9	8.8	3.9	11	4.1
Regional speed variance [m^2/s^2]	1.4	0.8	4.6	1.2	3.4	1.2
Central mean speed [m/s]	5.1	4.7	4.4	3.3	4.7	3.4
First ring mean speed [m/s]	6.3	6	4.6	4.6	4	4.6
Second ring mean speed [m/s]	7.8	7	8.2	6.3	8	6.1

lations exist using predictive control frameworks and including cooperation between regions. However, the new concept's initial formulation has been kept simple, and the centralized controller is only reactive. To make a fair comparison, we have implemented a reactive perimeter control strategy using both proportional and integral terms (PI control). The formulation comes from one of the first applications of perimeter control in multi-reservoir heterogeneous networks (Aboudolas and Geroliminis, 2013). We monitor the green time G_i of all signals that direct vehicles inside region i from its perimeter. Green time reductions are applied uniformly to all signals that belong to the same border.

$$G_i^t = G_{max} - K_p e_i^t - K_i \Delta t \sum_{k=0}^{t} e_i^k$$

K_p and K_i are the two parameters of the PI controller. G_{max} represents the maximum green time duration, which is applied when no congestion appears in a region. Let recall that $e_i{}^t = \max(0, u_i{}^* - u_i{}^t)$. In the Manhattan network, it corresponds to the original green time duration, i.e., 30 s. $G_i{}^t$ has a lower-bound $G_{min} = 10$ s to avoid gridlock creates by links with no exiting vehicles. When $G_i{}^t < G_{min}$, we apply an anti-windup process to the integral term (Bohn and Atherton, 1995) that stops accumulating errors during the period where the optimal control value $G_i{}^t$ is outside the predefined physical bounds. The control time horizon is set to 1 min, meaning that green times are updated at each signal cycle. All vehicles stick to their initial path assignment as there is no adaptive (en-route) choice model implemented in our simulator. Further development would have been required to add this feature.

We consider the two initial settings (shortest paths in distance or user equilibrium) for the demand scenario A. We also tested two different implementations for the perimeter control. The individual perimeter control uses the same partitioning in regions as the route guidance approach and independently control entry flows, i.e. intersection legs with vehicles that aim to enter. The centric perimeter control introduces a rough layer of cooperation. Initial regions are gathered into three: the central area is left alone while regions in the first and the second rings come together, see Fig. 14. In that latter case, only centric inflows are controlled; see arrows in Fig. 14b. Such an implementation mimics the classical nested centric network partitioning used in perimeter control.

The optimal parameter values have been determined based on extensive sensitivity analysis in each case (perimeter control type and initial loading). Table 3 presents the comparison results considering all the main indicators we used in the paper. We also monitor the overall mean speed in the central region and the two rings; see Fig. 14a below.

The results show that the perimeter control strategies underperform compared to the new concept. The travel time improvement (V_{ttt}) never exceeds 2.5%. However, they have fewer impacts on individuals as they do not increase travel distance (D_{up}) and significantly reduces the adverse effects on individual travel times (T_{loss}). The perimeter control strategies do not

change individual routes in our implementation, so no users should make an effort for the better good. Some studies have shown, e.g. (Ingole et al., 2020), that considering adaptative routing related to user equilibrium can significantly improve the overall system performances as it reduces vehicle queueing at the region gates. So, we can expect that the perimeter control strategies perform better in reality. Note that we did not expand our simulation framework to account for such behavior, as perimeter control is not the primary focus of this paper.

An important insight in Table 3 is that the regional speed variance is much lower when applying the new concept than both perimeter control strategies. It means that the new concept acts as expected and favors a more homogeneous distribution of vehicles inside the network. The main difference between the new concept and perimeter control strategies is that the mean speed is significantly higher in the first ring. With perimeter control, vehicles that have to cross the central region first queue in the first ring regions. The reactive implementation does not adjust the inflows from the second ring fast enough to counterbalance this effect. In short, congestion is propagating faster than the system perceives and reacts. It confirms the need for predictive methods to improve perimeter control strategies when the network is heavily loaded. It is undoubtedly a clear advantage of the optimal routing strategy. Even if the public avoidance maps are derived from a reactive control process, they have a broader spatial impact on vehicles, as they start adjusting their trips as soon as they enter the network. When congestion appears in the central region, perimeter control strategies first only reduce the inflows locally at the region gates. On the contrary, the optimal routing targets all vehicles that initially aim to cross this region, whatever their position in the network. In that sense, the optimal routing strategy better anticipates vehicle rebalancing in the network and better accommodates a rougher control framework. Again, considering adaptive routing combined with the perimeter control strategy will partly compensate for the observed effects. Still, it cannot compete with direct route guidance to users tailored for system optimum instead of user equilibrium.

Declaration of Competing Interest

No.

Acknowledgements

This study has received funding from the European Research Council (ERC) under the European Union's Horizon 2020 research and innovation program (grant agreement No 646592 – MAGnUM project).

References

Aboudolas, K., Geroliminis, N., 2013. Perimeter and boundary flow control in multi-reservoir heterogeneous networks. Transp. Res. Part B 55, 265–281.
Ambühl, L., Loder, A., Bliemer, M.C.J., Menendez, M., Axhausen, K.W., 2018. Introducing a *Re*-sampling methodology for the estimation of empirical macroscopic fundamental diagrams. Transp. Res. Record. 2678 (20), 239–248.
Ameli, M., Lebacque, J.P., Leclercq, L., 2020b. Simulation-based dynamic traffic assignment: meta-heuristic solution methods with parallel computing. Comput.-Aided Civil Infrastructure Engineering 35 (10), 1047–1062.
Ameli, M., Lebacque, L., Leclercq, L., 2020a. Cross-comparison of convergence algorithms to solve trip-based dynamic traffic assignment problems. Computer-Aided Civil Infrastruct. Eng. 35 (3), 219–240.
Ampountolas, K., Zheng, N., Geroliminis, N., 2017. Macroscopic modelling and robust control of bi-modal multi-region urban road networks. Transp. Res. Part B 104, 616–637.
Bohn, C., Atherton, D.P., 1995. An analysis package comparing pid anti-windup strategies. IEEE Syst. Mag. 15 (2), 34–40.
Chevallier, E., Leclercq, L., 2009. Do microscopic merging models reproduce the observed priority sharing ratio in congestion? Transp. Res. Part C 17 (3), 328–336.
Chevallier, E., Leclercq, L., 2008. A macroscopic single-lane roundabout model to account for insertion delays and o-d patterns. Comput.-Aided Civil Infrastruct. Eng. 23 (2), 104–115.
Ding, H., Guo, F., Zheng, X., Zhang, W., 2017. Traffic guidance–perimeter control coupled method for the congestion in a macro network. Transp. Res. Part C 81, 300–316.
Geroliminis, N., Haddad, J., Ramezani, M., 2013. Optimal perimeter control for two urban regions with macroscopic fundamental diagrams: a model predictive approach. IEEE Trans. ITS 14 (1), 348–359.
Haddad, J., 2017a. Optimal coupled and decoupled perimeter control in one-region cities. Control Eng. Pract.. 61, 134–148.
Haddad, J., 2017b. Optimal perimeter control synthesis for two urban regions with aggregate boundary queue dynamics. Transp. Res. Part B 96, 1–25.
Haddad, J., Mirkin, B., 2017. Coordinated distributed adaptive perimeter control for large-scale urban road networks. Transp. Res. Part C 77, 495–515.
Haddad, J., Shraiber, A., 2014. Robust perimeter control design for an urban region. Transp. Res. Part B 68, 315–332.
Hajiahmadi, M., Haddad, J., De Schutter, B., Geroliminis, N., 2015. Optimal hybrid perimeter and switching plans control for urban traffic networks. IEEE Trans. Control Syst. Technol. 23 (2), 464–478.
Ingole, D., Mariotte, G., Leclercq, L., 2020. Perimeter gating control and citywide dynamic user equilibrium: a macroscopic modeling framework. Transp. Res. Part C 111, 22–49.
Ji, Y., Geroliminis, N., 2012. On the spatial partitioning of urban transportation networks. Transp. Res. Part B 46 (10), 1639–1656.
Jian-Xin, X., Huang, D., Pindi., S., 2008. Optimal tuning of PID parameters using iterative learning approach. SICE J. Control Measur. Syst. Integrat. 1 (2), 143–154.
Kouvelas, A., Saeedmanesh, M., Geroliminis, N., 2017. Enhancing model-based feedback perimeter control with data-driven online adaptive optimization. Transp. Res. Part B 96, 26–45.
Keyvan-Ekbatani, M., Papageorgiou, M., Knoop, V.L., 2015a. Controller design for gating traffic control in presence of time-delay in urban road networks. Transp. Res. Part B 7 (6), 397–402.
Keyvan-Ekbatani, M., Yildirimoglu, M., Geroliminis, N., Papageorgiou, M., 2015b. Multiple concentric gating traffic control in large-scale urban networks. IEEE Trans. ITS 16 (4), 2141–2154.
Keyvan-Ekbatani, M., Papageorgiou, M., Papamichail, I., 2013. Urban congestion gating control based on reduced operational network fundamental diagrams. Transp. Res. Part C 33, 74–87.
Keyvan-Ekbatani, M., Kouvelas, A., Papamichail, I., Papageorgiou, M., 2012. Exploiting the fundamental diagram of urban networks for feedback-based gating. Transp. Res. Part B 46 (10), 1393–1403.

Laval, J.A., Leclercq, L., 2008. Microscopic modeling of the relaxation phenomenon using a macroscopic lane-changing model. Transp. Res. Part B 42 (6), 511–522.
Leclercq, L., Paipuri, M., 2019. Macroscopic traffic dynamics under fast-varying demand. Transp. Sci. 53 (6), 1526–1545.
Leclercq, L., Chiabaut, N., Trinquier, B., 2014. Macroscopic fundamental diagrams: a cross-comparison of estimation methods. Transp. Res. Part B 62, 1–12.
Leclercq, L., Laval, J.A., Chevallier, E., 2007. The Lagrangian coordinates and what it means for first order traffic flow models. In: Allsop, R.E., Bell, M.G.H., Heydecker, B.G. (Eds.), Proceedings of the 17th International Symposium on Transportation and Traffic Theory, London. Elsevier, pp. 735–753.
Leclercq, L., 2007. Bounded acceleration close to fixed and moving bottlenecks. Transp. Res. Part B 41 (3), 309–319.
Lopez, C., Leclercq, L., Krishnakumari, P., Chiabaut, N., Van Lint, H., 2017. Revealing the day-to-day regularity of urban congestion patterns with 3D speed maps. Sci Rep 7 (1), 14029.
Munoz, J., Laval, J.A., 2006. System optimum dynamic traffic assignment graphical solution method for a congested freeway and one destination. Transp. Res. Part B 40 (1), 1–15.
Nie, W., Cassidy, M., 2019. City-wide traffic control: modelling impacts of cordon queues. Transp. Res. Part C 113, 164–175.
Olfati-Saber, R., Fax, J.A., Murray, R.M., 2007. Consensus and cooperation in networked multi-agent systems. Proc. IEEE 95 (1), 215–233.
Ramezani, M., Haddad, J., Geroliminis, N., 2015. Dynamics of heterogeneity in urban networks: aggregated traffic modeling and hierarchical control. Transp. Res. Part B 74, 1–19.
Saeedmanesh, M., Geroliminis, N., 2017. Dynamic clustering and propagation of congestion in heterogeneously congested urban traffic networks. Transp. Res. Part B 105, 193–211.
Saeedmanesh, M., Geroliminis, N., 2016. Clustering of heterogeneous networks with directional flows based on “Snake” similarities. Transp. Res. Part B 91, 250–269.
Sirmatel, I.I., Geroliminis, N., 2018. Economic model predictive control of large-scale urban road networks via perimeter control and regional route guidance. IEEE Trans. ITS 19 (4), 1112–1121.
Van Erp, P.B., Knoop, V.L., Hoogendoorn, S.P., 2017. Macroscopic traffic state estimation: understanding traffic sensing data-based estimation errors. J. Adv. Transp., 5730648.
Wardrop, J.G., 1952. Some theoretical aspects of road traffic research. Proc. Inst. Civil Eng. 1 (3), 325–362.
Yang, K., Zheng, N., Menendez, M., 2016. Multi-scale perimeter control approach in a connected-vehicle environment. Transp. Res. Part C 94, 32–49.
Yildirimoglu, M., Sirmatel, I.I., Geroliminis, N., 2018. Hierarchical control of heterogeneous large-scale urban road networks via path assignment and regional route guidance. Transp. Res. Part B 118, 106–123.
Yildirimoglu, M., Ramezani, M., Geroliminis, N., 2015. Equilibrium analysis and route guidance in large-scale networks with MFD dynamics. Transp. Res. Part C 59, 404–420.